

ANL-HEP-CP-01-10
June 14, 2019

HERA Small- x and/or Diffraction

RIK YOSHIDA

ON BEHALF OF THE ZEUS AND H1 COLLABORATIONS

Argonne National Laboratory

9700 S. Cass Ave, Argonne, Illinois 60439, USA

Recent HERA data on small- x structure functions as well as DIS diffraction and diffractive vector meson production are presented. The relationship between these processes and possible indications of dynamics beyond the DGLAP formalism are discussed.

PRESENTED AT

5th International Symposium on Radiative Corrections
(RADCOR-2000)

Carmel CA, USA, 11–15 September, 2000

1 Proton Structure Function F_2 at Small- x

1.1 Deep Inelastic Scattering and F_2

Deep Inelastic Scattering (DIS) of electrons (or positrons) with a proton is shown in Figure 1. The reaction proceeds through the exchange of a virtual boson; in the kinematic range covered in this talk, only photon exchange is important. The reaction can be described completely by two kinematic variables chosen to be the four-momentum transfer squared, $Q^2 = -q^2$ (see Figure 1), and the Bjorken variable, x . In the Quark Parton Model, x is the fraction of the initial proton momentum carried by the struck parton.

The DIS cross-section factorizes into a short-distance part which is the partonic cross-section, $\hat{\sigma}$, which can be calculated perturbatively in QCD, and a long-distance non-perturbative part, the parton densities, f .

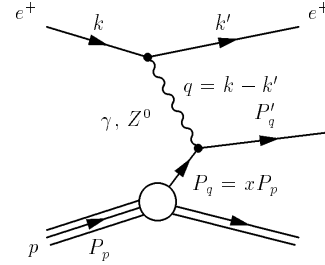


Figure 1: Collision of electron (positron), e^\pm , of four-momentum k with a proton, p , of four-momentum P_p .

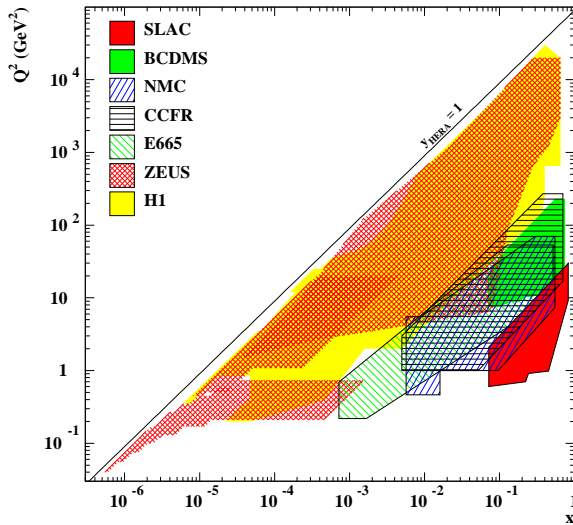


Figure 2: The kinematic region in which the proton F_2 has been measured. H1 and ZEUS are the experiments at the HERA ep collider.

At sufficiently high Q^2 , the parton densities, f , obey the DGLAP equation [1], which is written schematically as,

$$\frac{\partial f}{\partial \ln Q^2} \sim f \otimes P, \quad (1)$$

where P are the splitting functions that describe the branching of quarks and gluons, and \otimes symbolizes a convolution.

The DIS differential cross-section can be written in terms of the proton structure function F_2 as

$$\frac{d\sigma^2}{dx dQ^2} = \frac{2\pi\alpha^2}{xQ^4} (1 + (1-y)^2) F_2(x, Q^2), \quad (2)$$

where $y = Q^2/xs$ is the inelasticity parameter, and s is the CMS energy squared of the ep collision. The longitudinal structure function F_L and the effects of Z^0 exchange have been neglected in Equation (2).

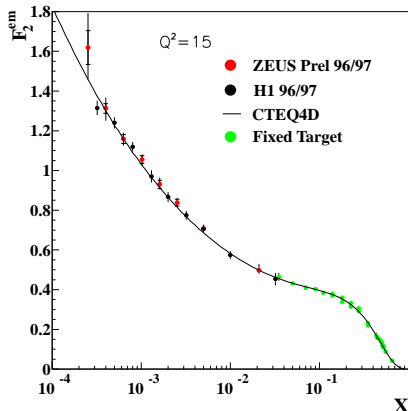


Figure 3: World's data on F_2 at $Q^2 = 15$ GeV^2 as a function of x . The solid line is a DGLAP fit by the CTEQ group [2].

$x^{-\lambda}$, then λ falls as a function of Q^2 from about 0.4 to 0.1 as Q^2 falls from 200 GeV^2 to 1 GeV^2 . At Q^2 of 10 GeV^2 , λ is about 0.2 (Figure 4) [5, 6].

The naive physical interpretation of the small- x rise of F_2 is that it is caused by more and more gluons (and thus sea-quarks) being present at smaller and smaller fractional momenta values, i.e. x .

The scaling violations of F_2 (i.e. the Q^2 dependence of F_2 at fixed x , as seen in Figure 5) at low x are related, in Leading Order (LO) DGLAP, simply to the gluon density of the proton [7],

$$\frac{\partial F_2(x/2, Q^2)}{\partial \ln Q^2} \propto \alpha_s x g(x, Q^2). \quad (4)$$

In Next-to-LO (NLO) DGLAP, the simple relationship of Equation (4) no longer holds. However, the gluon density may be extracted from the NLO DGLAP fits to F_2 .

As an example of such fits, the one made by the H1 collaboration is briefly described [3].

The fit is made to the H1 data and the BCDMS μp data at $Q^2 > 3.5 \text{ GeV}^2$. The flavor decomposition of F_2 into the gluon xg , the valence component V , and the sea

At leading order,

$$F_2(x, Q^2) = x \sum_q e_q^2 (q(x, Q^2) + \bar{q}(x, Q^2)), \quad (3)$$

where q , \bar{q} are the quark and antiquark distributions, respectively.

Figure 2 shows the x and Q^2 range of the currently available measurements of F_2 . At the HERA ep collider, with \sqrt{s} of about 300 GeV , x and Q^2 can be varied over six orders of magnitude. Of particular relevance to this talk is the region of smallest x , which is probed only at HERA.

The measurements of F_2 at HERA show that the structure function rises steeply at small x (see Figure 3) [3, 4].

If F_2 at $x < 0.1$ is parameterized as \propto

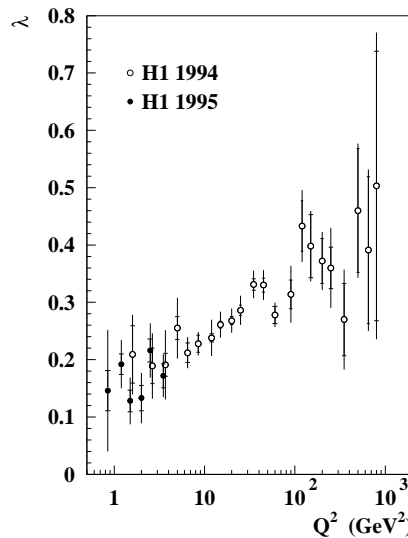


Figure 4: The parameter λ of the x dependence of F_2 . See text and ref. [5].

component A is done in such a way as to allow the use of proton data only and avoid the deuteron data which introduces nuclear-correction uncertainties.

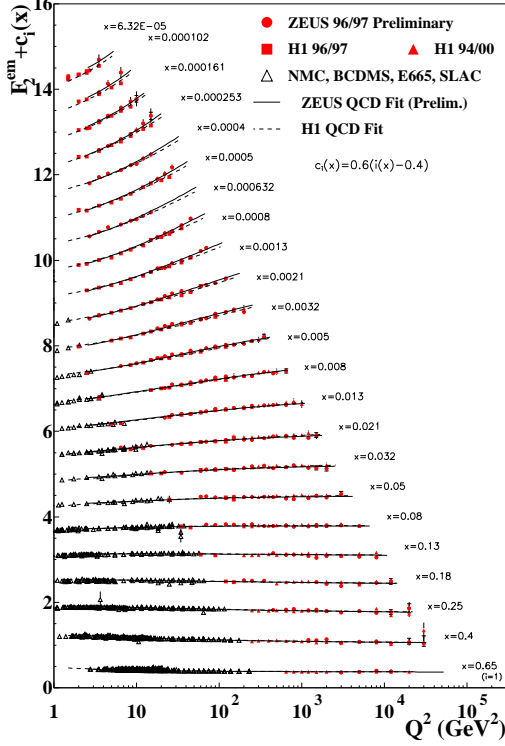


Figure 5: Proton F_2 for fixed x as functions of Q^2 . A constant, c_i , has been added to F_2 in order to make all of the points visible.

$$W \approx \sqrt{Q^2/x}.$$

The total virtual-photon proton cross-section, at small- x , can be written in terms of F_2 as

$$\sigma_{tot}^{\gamma^*p}(W^2, Q^2) = \frac{4\pi^2\alpha}{Q^2} F_2(x, Q^2). \quad (5)$$

For fixed Q^2 , $F_2 \propto x^{-\lambda}$ implies $\sigma_{tot}^{\gamma^*p} \propto W^{2\lambda}$. The structure function F_2 must vanish as Q^2 , for fixed W , as Q^2 approaches 0, by conservation of EM current. At $Q^2 = 0$ (photoproduction), the cross-section, $\sigma_{tot}(W)$, is described by Regge phenomenology, and is known to agree with the universal hadron-hadron cross-section behavior at high energies, $\sigma_{tot}(W) \propto W^{2(\alpha_{\mathbb{P}}-1)}$ [8]. The Pomeron intercept $\alpha_{\mathbb{P}}$ has the value 1.08 [9]. Thus at $Q^2 = 0$, $\sigma_{tot}(W) \propto W^{0.16}$, in contrast to $\sigma_{tot}^{\gamma^*p}(W^2, Q^2) \propto W^{0.4}$ at $Q^2 \approx 10 \text{ GeV}^2$.

The xg , V , and A distributions are parameterized in the form $ax^b(1-x)^c \times (1+d\sqrt{x}+ex)$. The momentum sum rule is imposed leading to 16 parameters to be fitted including α_s . The fits are made by employing Equations (1) and (3) (in their NLO versions).

Figure 6 shows the gluon density extracted from the fit. In keeping with the naive expectation of a gluon-driven F_2 , the gluons also rise steeply at low x . As Q^2 falls, the steepness of the gluon also becomes less, as in the case of F_2 itself.

1.2 DIS and $\sigma_{tot}^{\gamma^*p}$

Figure 2 shows that due to the kinematic limit at HERA, the measurements of F_2 at the smallest x values of 10^{-6} – 10^{-5} correspond to rather small values of Q^2 , well below 1 GeV^2 . In this kinematic range, it is appropriate to describe DIS in the hadronic language of a collision between a virtual photon and a proton. The appropriate variable, in this case, becomes the virtual-photon proton CMS energy,

Figure 7 shows the measured F_2 at fixed $y = W^2/s$ down to the Q^2 value of 0.04 GeV^2 . F_2 begins to fall as Q^2 below $Q^2 < 1 \text{ GeV}^2$. The dashed line is a Regge inspired fit in the form $F_2(x, Q^2) = (\frac{Q^2}{4\pi^2\alpha}) \cdot (\frac{M_0^2}{M_0^2 + Q^2}) \cdot (A_{\text{R}} \cdot (W^2)^{\alpha_{\text{R}}-1} + A_{\text{P}} \cdot (W^2)^{\alpha_{\text{P}}-1})$. The α_{P} value of 1.1 gives a good fit. This is consistent with the value of Pomeron intercept discussed above [6].

Also shown in Figure 7 is a NLO DGLAP fit which gives a good description of the data from high Q^2 down to about 1 GeV^2 .

1.3 Beyond DGLAP?

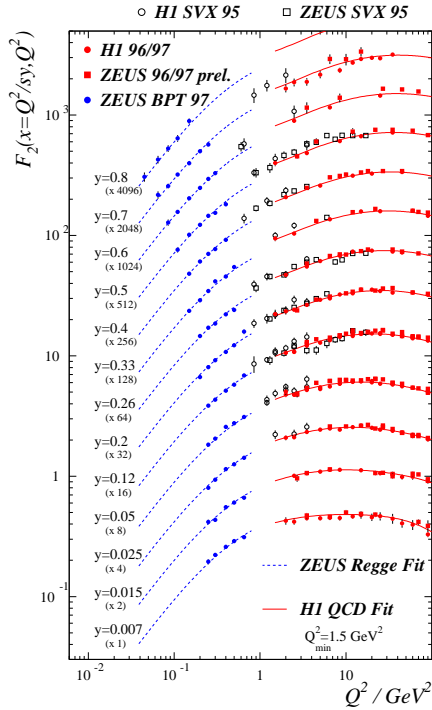


Figure 7: F_2 as a function of Q^2 . The lines are Regge and pQCD fits.

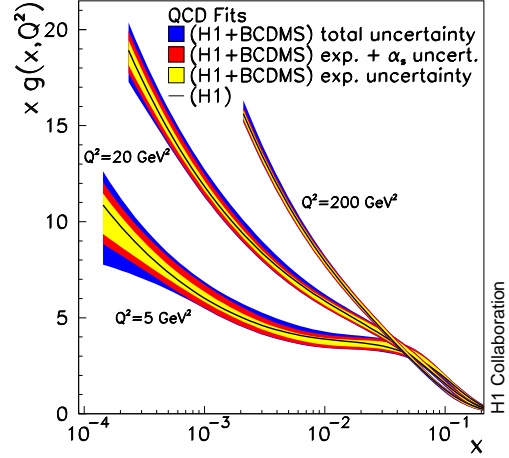


Figure 6: The gluon distribution extracted by the H1 Collab. See [3] for details.

The interest in small- x physics is that the partons under study are the result of a large number of QCD branching processes. The evolution of the number of partons over a wide kinematic range in x and Q^2 should be sensitive to the applicability of different perturbative approximations of QCD.

Figure 8 shows the qualitative expectation of applicability of various pQCD approaches. DGLAP is a resummation of terms proportional to $(\ln Q^2)$ and is expected to hold in the region of large Q^2 . BFKL [10] is a resummation of terms proportional to $(\ln 1/x)$ and, while the stability of the perturbative expansion is in some doubt [11], it is expected to hold in the region of small x . The CCFM [12] equation incorporates both $(\ln 1/x)$ and $(\ln Q^2)$ terms.

At small enough x , the density of partons should become sufficiently large so that the interactions between them become important. This boundary is marked in Figure 8 by the line labeled “critical line”. The GLR equations [13] attempt to take these saturation, or shadowing, effects into account.

It has been shown above that the DGLAP formalism is able to describe the currently available F_2 data down to 1 GeV^2 and x of 10^{-5} in apparent contradiction to Figure 8, at least with the $1/x$ scale numbers as drawn.

On the other hand, there have also been successful fits to a wide range of F_2 data using formalisms that incorporate the $(\ln 1/x)$ terms as well as the $(\ln Q^2)$ terms [14, 15].

In search of clarification, we turn next to the phenomenon of DIS diffraction, and vector meson production, before returning to consider if there are any indications in the F_2 data for dynamics beyond DGLAP.

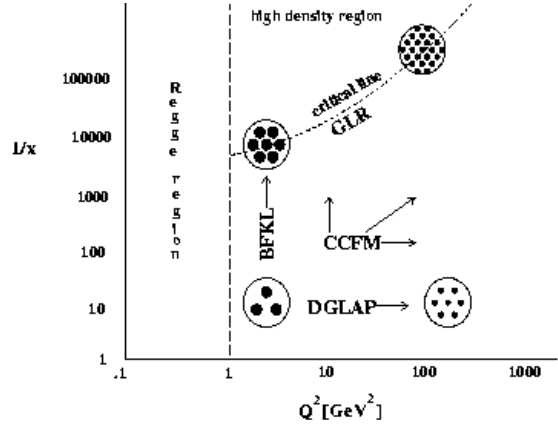


Figure 8: Schematic diagram of the applicability of different pQCD approximations.

2 Diffraction in DIS

One of the striking results from HERA is the presence of diffractive events in DIS [16, 17]. About 10% of all DIS events have a gap in particle emission between the final-state proton, or a low mass state, which travels down the beampipe, and the system X , which is measured in the detector (Figure 9). Such a reaction is usually described as an exchange of a colorless object, generically called the Pomeron (\mathbb{P}).

In order to describe diffractive DIS, two kinematic variables in addition to x and Q^2 are needed. These are t , which is the momentum transfer at the proton vertex and $x_{\mathbb{P}}$, which is the fractional momentum of the proton carried by the Pomeron. Another useful variable is $\beta = x/x_{\mathbb{P}}$, which has an interpretation as the fractional momentum of the Pomeron carried by the struck parton (i.e. the Pomeron analogue of x for the proton).

Any perturbative description of diffractive DIS must go beyond the simplest DGLAP picture; the lack of color connections between the system X and the proton must mean that at least two gluons are

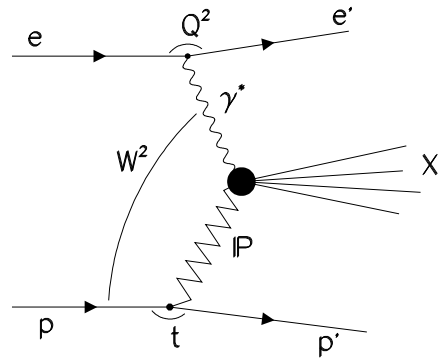


Figure 9: Diffractive DIS scattering.

exchanged. It is then interesting to investigate the connection between the high gluon densities implied by the F_2 measurements and the phenomenon of DIS diffraction.

2.1 Diffractive Factorization and Pomeron Structure

The diffractive cross-section, in analogy with the total cross-section, is written in terms of the diffractive structure function F_2^D as

$$\frac{d^3\sigma^D}{d\beta dQ^2 dx_{\mathbb{P}}} = \frac{2\pi\alpha^2}{\beta Q^4} (1 + (1-y)^2) \times F_2^{D(3)}(\beta, Q^2, x_{\mathbb{P}}). \quad (6)$$

The cross-section has been integrated over t . It has been proven that F_2^D factorizes into a long and a short distance contributions, as does the inclusive F_2 , i.e. $F_2^D \sim f^D \otimes \hat{\sigma}$ where $\hat{\sigma}$ are the usual pQCD hard cross-sections and f^D are the diffractive parton densities, which obey the usual DGLAP equations, and are universal [19]. By knowing f^D , we can calculate any diffractive DIS final state such as charm or jet production.

The diffractive parton densities are functions of four variables: $x_{\mathbb{P}}$, t , β and Q^2 . However, the DGLAP evolution only concerns the variables x (or β) and Q^2 . If, for all relevant f^D 's, the $x_{\mathbb{P}}$ and t dependences decouple from the β and Q^2 dependence, *and* if the $x_{\mathbb{P}}$ and t dependences are the *same* for all relevant partons, then we arrive at what is known as Regge factorization [20],

$$F_2^D(x_{\mathbb{P}}, t, Q^2, \beta) = f(x_{\mathbb{P}}, t) \cdot F_2^{\mathbb{P}}(\beta, Q^2). \quad (7)$$

In this case $f(x_{\mathbb{P}}, t)$ can be interpreted as the flux factor of the Pomeron, and $F_2^{\mathbb{P}}$ as the structure function of the Pomeron. In this case DGLAP analysis of $F_2^{\mathbb{P}}$ becomes meaningful. It is a remarkable experimental fact that Regge factorization, which is not required by the diffractive factorization theorem, apparently holds over a large part of the measured phase-space, and that the flux factor, $f(x_{\mathbb{P}}, t)$, has approximately the form expected by Regge theory of $1/x_{\mathbb{P}}^{2\bar{\alpha}_{\mathbb{P}}-1}$ [16, 17] (see also Figure 17a).

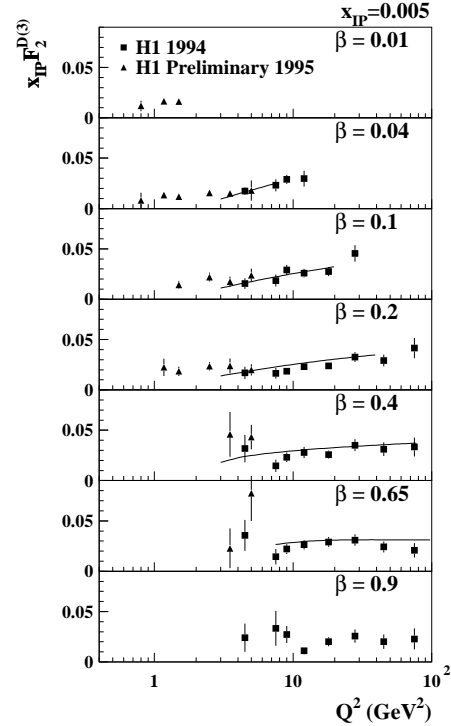


Figure 10: The diffractive structure function for a bin of $x_{\mathbb{P}}$ measured by the H1 Collab. See text.

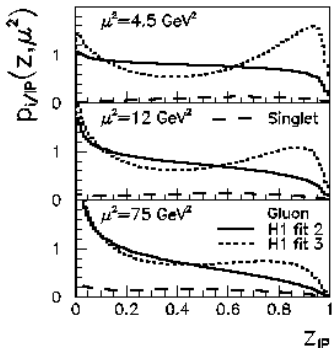


Figure 11: The parton distribution, P , of the Pomeron extracted by the H1 Collab. See text.

the DGLAP analysis can indeed be used to describe the dijet cross-section in diffractive events (Figure 12). The jet measurement favors the parton distributions labelled “fit 2” in Figure 11.

2.2 Diffraction and F_2 at Small- x

While the analyses based on diffractive factorization have been very successful and powerful, the question of the origin of the phenomenon of DIS diffraction remains unanswered. Furthermore, the relationship between the Pomeron structure and the proton structure is not clear.

Figure 13 shows the ratio, for fixed Q^2 , of the DIS diffractive cross section to the total DIS cross-section as measured by the ZEUS collaboration. Although a cut has been made in the mass of the diffractive system, M_X , the conclusion is independent of M_X : the ratio is flat as a function of W or, equivalently for fixed Q^2 , of x [16]. The flatness of the ratio implies that the energy dependence of DIS diffraction is the same as that of inclusive DIS, i.e. $\propto W^{0.4}$ at $Q^2 \approx 10 \text{ GeV}^2$.

This result is surprising from several points of view. A naive expectation from the optical theorem would lead to diffractive cross sections

Figure 10 shows the measurements of $F_2^{D(3)}$ by the H1 collaboration for x_{IP} of 0.005 [17, 18]. The lines are the results of the DGLAP analysis. The resulting parton distributions in the Pomeron is shown in Figure 11.

The analysis finds two stable solutions, one of which (dotted line) favors a rather large amount of gluons at $z_{\text{IP}} = 1$, and the second which does not (solid line). The fractional momentum carried by the parton in the Pomeron is denoted by z_{IP} , and the renormalization and factorization scale by μ .

The recent measurement by H1 of dijet production in diffraction [21] shows that the Pomeron parton distributions extracted from

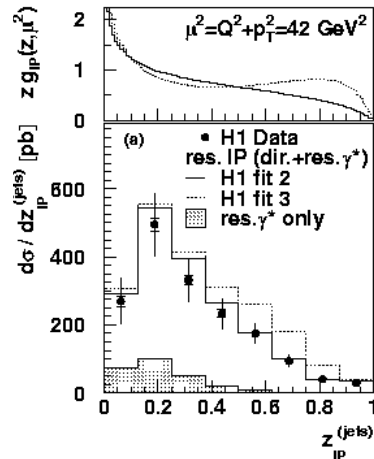


Figure 12: Dijet cross-section for diffractive events compared to predictions based on the gluon momentum distribution of the Pomeron, $z g_{\text{IP}}$. See text and ref [21].

that rise twice as fast as the inclusive one. In other words, if the rise of the inclusive cross-section is driven by a gluon density that rises as $x^{-\lambda}$ (or $W^{2\lambda}$), then for diffractive process that needs to couple to at least two gluons, the cross-section should rise as $x^{-2\lambda}$. At the same time, the energy dependence of the diffractive cross-section also contradicts Regge phenomenology, which expects an energy dependence of $W^{0.25-0.3}$.

The lines in Figure 13 that describe the data qualitatively are from the dipole model of Golec-Biernat and Wüsthoff [22, 23], briefly described below.

2.3 Impact Parameter Space (or Dipole) Models

The infinite momentum frame of DIS, which is appropriate for the DGLAP formalism, is obviously not the only possible frame of reference. In the impact parameter, or dipole, formalism, the appropriate frame of reference is that in which the virtual photon dissociates into a quark-anti quark pair (or a more complicated state), which forms a color dipole which collides with the proton (Figure 14).

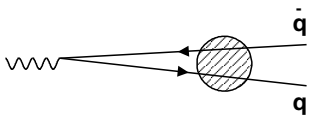


Figure 14: Color dipole picture of DIS

as r^2 in keeping with the behavior of perturbative QCD. At large r , $\hat{\sigma}_{dipole}$ becomes constant to preserve unitarity. The saturation of the dipole cross-section can be qualitatively shown to correspond to the saturation of partons in the proton [25].

In the model, the point at which the r^2 dependence of the cross-section changes to the constant behavior depends on the density of the partons in the proton. Specifically, a parameter, $R_0 \sim 1/xg(x) \sim x^\lambda$, which can be interpreted as the separation of

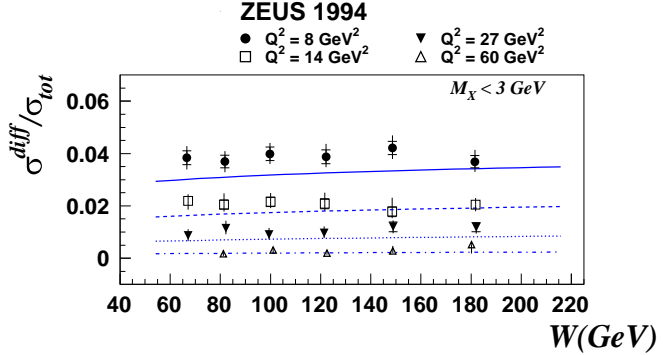


Figure 13: The ratio of diffractive to total DIS cross-section. The data have been binned in Q^2 and a cut on the mass of the state X , $M_X < 3$ GeV has been made.

The description of the interaction of this color dipole with the proton distinguishes the various models of this type that have been proposed [24]. In this presentation, a particularly simple model due to Golec-Biernat and Wüsthoff (GB&W) will be described.

In the GB&W model, the cross-section of the dipole, $\hat{\sigma}_{dipole}$, with the proton is modeled simply as a function that smoothly interpolates between two limits (Figure 15); at small dipole radius, r , $\hat{\sigma}_{dipole}$ increases

partons in the proton, is introduced. When $r \ll R_0$, $\hat{\sigma}_{dipole}$ is in the “pQCD” region, while when $r \gg R_0$, it is in the saturation region (Figure 16a and 16b, respectively).

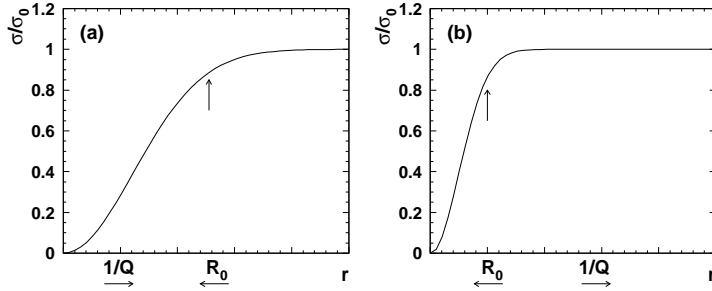


Figure 15: The dipole cross-section of the GB&W model for (a) the case of small dipole radius and (b) large dipole radius.

The dipole radius, r , enters through the wave function of the virtual photon, Ψ_γ , and the diffractive cross-section is written, up to a t dependence, as,

$$\sigma^D \propto \int d^2r \int dz \times |\Psi_\gamma(z, r)|^2 \hat{\sigma}_{dipole}^2(x, r), \quad (8)$$

where z is the fractional momentum of one of the

quarks in the dipole.

The diffractive cross-section is explicitly related to the total cross-section, which is,

$$\sigma_{tot} \propto \int d^2r \int dz |\Psi_\gamma(z, r)|^2 \hat{\sigma}_{dipole}(x, r). \quad (9)$$

The fact that σ^D/σ_{tot} is constant as a function of W (or x), as shown in Figure 13, can be shown to occur only if the dipole cross-section is being probed in these processes beyond the small r region into the saturation region. The implication of this for the total cross-section will be discussed below.

In Figure 17a, the measurements of F_2^D , this time from the ZEUS collaboration, are shown along with the prediction of the GB&W model. There is qualitative agreement. Figure 17b shows the recent measurement of F_2^D at very low Q^2 [26]. The GB&W model again describes the data qualitatively.

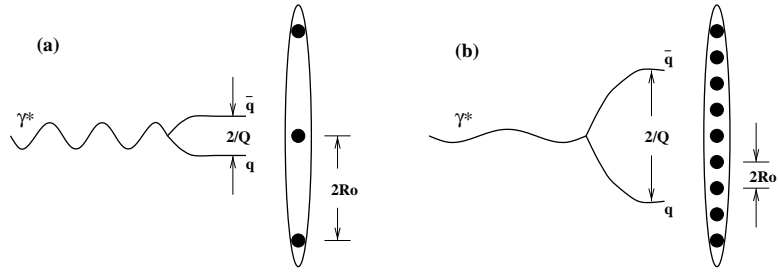


Figure 16: Schematic representation of the GB&W model. The characteristic radius of the dipole is proportional to the Q^2 of the virtual photon, γ^* . The parameter R_0 corresponds to the separation of the partons within the proton. The relative size of r and R_0 determines the behavior of the dipole cross-section.

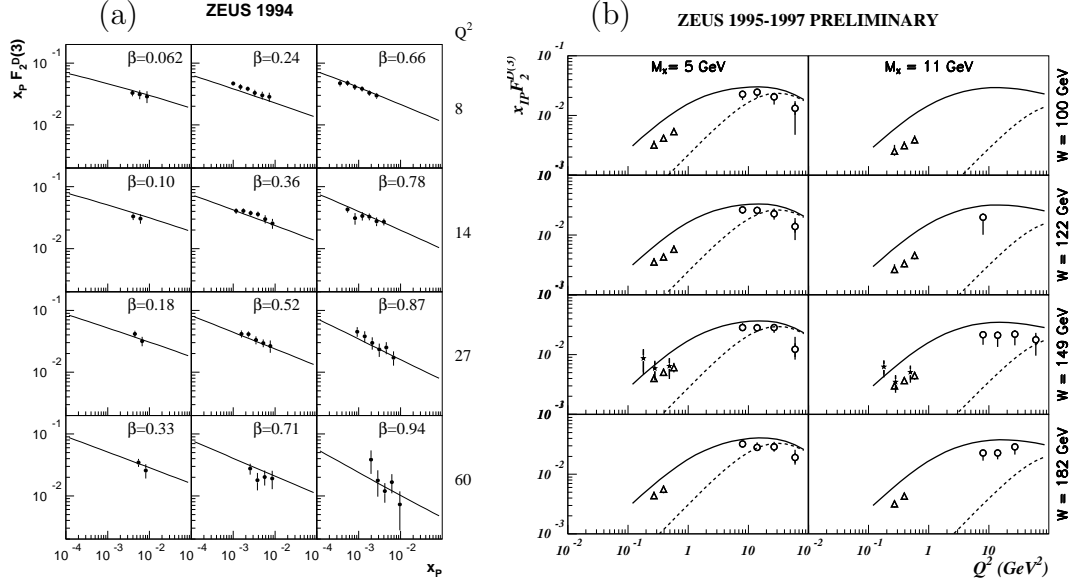


Figure 17: GB&W model (solid lines) compared to $x_P F_2^D(3)$ measurements. See text and refs [16, 23, 26].

3 Diffractive Vector Meson Production

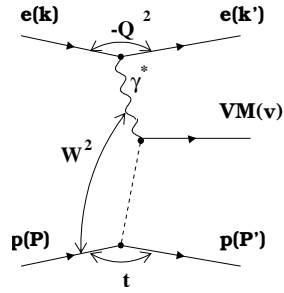


Figure 18: Diffractive VM production.

tion, i.e. $W^{2(\alpha_P-1)} \approx W^{0.16}$.

- The total virtual-photon proton cross-section, $\sigma_{tot}^{\gamma^*p}$, at $Q^2 \approx 10$ GeV² increases approximately as $W^{0.4}$, corresponding to F_2 rising as $x^{-0.2}$.
- The diffractive DIS cross-section, σ^D , has approximately the same energy dependence as $\sigma_{tot}^{\gamma^*p}$, i.e. increases as $W^{0.4}$ at $Q^2 \approx 10$ GeV².

The exclusive production of vector mesons (VM) in DIS is a process which is closely related to DIS inclusive diffraction. As seen in Figure 18, the final state X in Figure 9 is replaced by a vector meson. Let us review the energy dependences of the processes we have discussed so far:

- The total real photoproduction cross-section, $\sigma_{tot}^{\gamma p}$, increases in accordance with the Regge expectation

The energy dependence of exclusive vector meson production at $Q^2 = 0$ (photoproduction) is summarized in Figure 19. While the production of light vector mesons, ρ , ϕ and ω , have a weak energy dependence consistent with Regge expectations, the J/ψ production cross-section rises rapidly with energy, as $W^{0.8}$, i.e. twice as fast as $\sigma_{tot}^{\gamma^*p}$, at $Q^2 \approx 10 \text{ GeV}^2$. It is the fastest energy dependence of the processes discussed so far [27, 28].

The Q^2 dependence of the J/ψ production cross-section has been studied, but is still statistics limited. There is no evidence for a change of the energy dependence up to Q^2 of 15 GeV^2 [29].

The Q^2 dependence of ρ production cross-section is shown in Figure 20 [30], which shows δ , as obtained from a fit to the form W^δ , as a function of Q^2 . The energy dependence clearly rises as a function of Q^2 , although the precise form is not yet clear from the limited statistics.

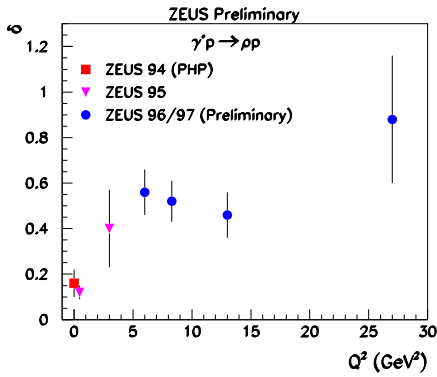


Figure 20: The energy dependence of ρ production as a function of Q^2 .

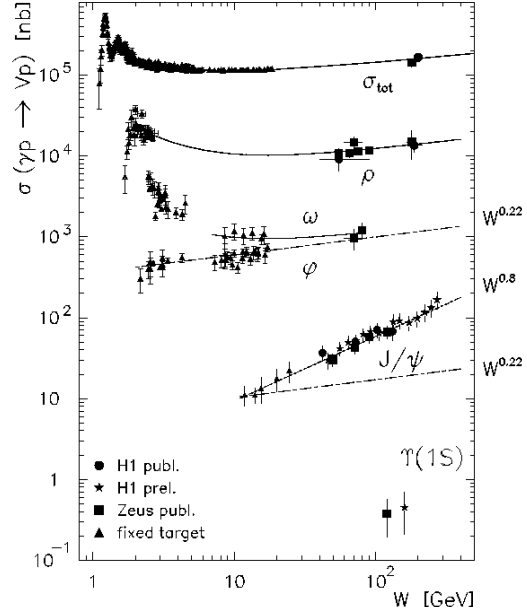


Figure 19: The W dependence of diffractive VM photoproduction.

In Figure 21, δ for various species of vector mesons has been plotted as a function of $Q^2 + M_{VM}^2$, where M_{VM} is the mass of the vector meson. While the statistics are still limited, the data are consistent with a scaling of δ with $Q^2 + M_{VM}^2$. If we recall that $\delta = 2\lambda$ (see Section 1.2), we can compare the energy dependence of vector meson production with that of inclusive DIS.

Comparing Figure 21 with Figure 4 which shows λ extracted from fits to F_2 to the form $x^{-\lambda}$ for $x < 0.1$, it can be seen that $\lambda_{(VM)}(Q^2 + M_{VM}^2) \approx 2\lambda_{(F_2)}(Q^2)$. This means that the vector meson production has an energy dependence at $Q^2 + M_{VM}^2$ which is twice as fast as that of the inclusive DIS cross-section at Q^2 .

The ratio of cross-sections of different species of vector mesons to the ρ meson is shown in Figure 22 as a function of $Q^2 + M_{VM}^2$. The ratio is flat as a function of $Q^2 + M_{VM}^2$ and is consistent with the ratios $\rho : \omega : \phi : J/\psi$ being 9:1:2:8. Such ratios are expected from the coupling of a photon to a vector meson, f_{VM}^2 , from simple charge counting of the quark content of the vector mesons.

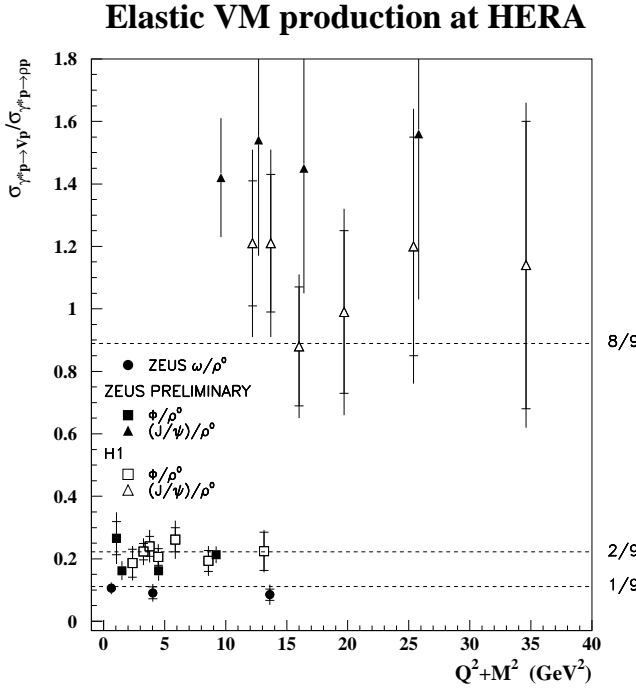


Figure 22: Ratios of diffractive VM production cross-sections to diffractive ρ production cross-section, as a function of $Q^2 + M_{VM}^2$.

ing $Q^2 + M_{VM}^2$. This is an indication that $Q^2 + M_{VM}^2$ is indeed giving the effective radius of the interaction, and thus the radius of the vector meson, or the color dipole.

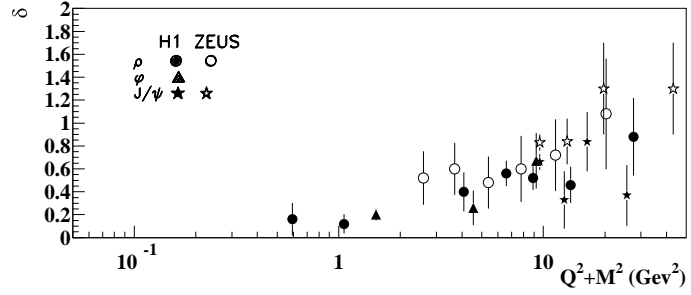


Figure 21: Energy dependence parameter δ for different VM's plotted as a function of $Q^2 + M_{VM}^2$.

In the Vector Meson Dominance Model (VDM) of the production of vector mesons in photon (or virtual photon) proton collisions, the cross-section is given as $\sigma_{VM} = f_{VM}^2 \cdot \sigma_{VMp}$, where σ_{VMp} is the vector-meson proton cross-section. The fact that the ratio of the cross-sections is given by f_{VM}^2 implies that σ_{VMp} for different species of vector mesons scales as $Q^2 + M_{VM}^2$. In the context of color dipole models, the implication is that $Q^2 + M_{VM}^2$ gives a measure of the radius, r , of the color dipole, which is the primary variable on which the cross-section depends.

Figure 23 shows the values of the t slope, b , where the vector meson cross-sections are parameterized as $d\sigma_{VM}/d|t| \propto e^{-b|t|}$. The parameter b is plotted as a function of $Q^2 + M_{VM}^2$. Within the statistical accuracy of the measurements, b scales with $Q^2 + M_{VM}^2$ and decreases with increasing

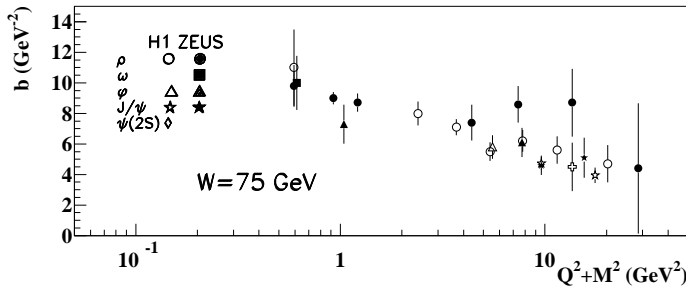


Figure 23: The slope dependence parameter b for different VM's plotted as a function of $Q^2 + M_{VM}^2$.

Ψ_γ , is not a well known quantity. Recently, evaluation of vector meson production in the context of Equation (10) and the dipole cross-section, $\hat{\sigma}_{dipole}$, from the GB&W model has been made [31]. Simple wave-functions for the vector mesons were chosen. The results reproduce the elastic J/ψ cross-section and their energy dependence very well. For the lighter mesons, ϕ and ρ , the calculations fail to give a good description of the magnitude of the cross-sections. However, the steepening of the energy dependence with increasing Q^2 (Figure 20) is well reproduced.

4 F_2 at Small- x Revisited

In the first part of this presentation, it was stated that the proton F_2 measured so far at HERA and elsewhere is well described by fits using DGLAP equations above Q^2 of 1 GeV², and a model combining Regge theory and Vector Meson Dominance has been shown to work well below 1 GeV².

The dipole model description of the total DIS cross-section (or F_2) is given in Equation (9). Currently the formal connection between the DGLAP interpretation and the dipole models is far from clear [25, 32, 33]. However many dipole models, in particular the GB&W model, describe the dynamics of cross-section saturation which goes beyond the physics of the DGLAP picture. Thus, it is appropriate to revisit the inclusive DIS data and ask if there are any indications of behavior beyond DGLAP, even though the DGLAP fits are successful.

The DGLAP evolution equations, at low x and at LO, imply that the partial derivative of F_2 with respect to $(\ln Q^2)$ is proportional to $xg(x, Q^2)$, the gluon momentum density of the proton (Equation (4)). On the other hand, at sufficiently low Q^2 , F_2 must vanish as Q^2 from current conservation, a behavior built into the GB&W model but not in the DGLAP formulation of DIS:

$$\frac{\partial F_2}{\partial \log Q^2} \propto Q^2 \sigma_0. \quad (11)$$

The cross-section for diffractive vector meson production can be written in the color dipole model as,

$$\sigma_{VM} \sim \left| \int dz \int d^2 r \Psi_{VM} \times \hat{\sigma}_{dipole} \Psi_\gamma \right|^2, \quad (10)$$

where Ψ_{VM} is the wave function of the vector meson, which, in contrast to the virtual photon wave function,

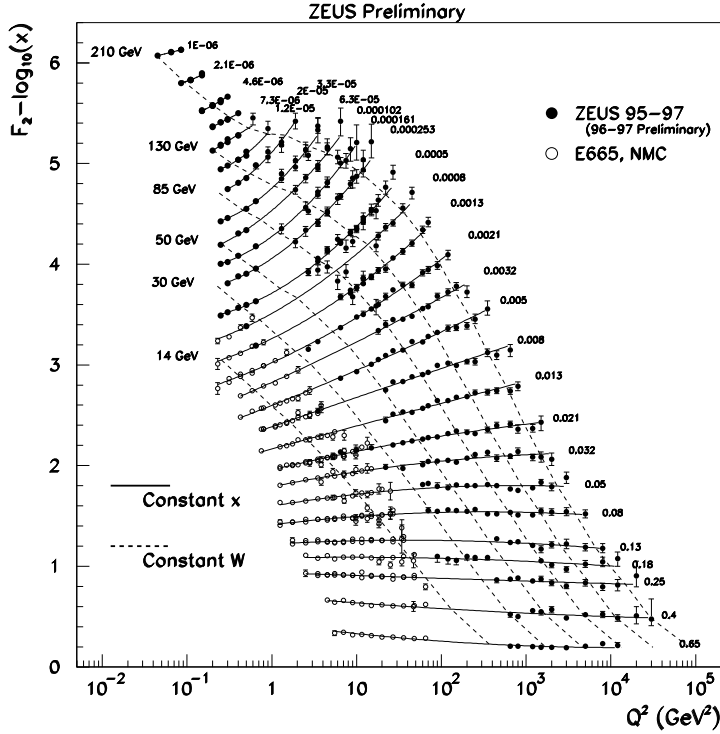


Figure 24: F_2 measurements in bins of x as a function of Q^2 . The solid lines are the results of the fits described in the text.

the nature of the transition [34].

Figure 24 shows recent measurements of F_2 from the ZEUS collaboration along with the fixed target measurements [35] from the NMC and the E665 collaborations. F_2 is shown as a function of Q^2 for bins of fixed x . Where necessary, the measurements have been interpolated to the appropriate values of x using the ALLM parameterization [36]. The F_2 in each bin of fixed x is offset by an additive factor of $(-\log_{10} x)$ to ensure that the vertical separation between the bins is monotonic in x . Therefore, at low x , the line connecting $F_2 - \log_{10} x$ at constant W would be a straight line, as a function of $\log_{10} Q^2$, if F_2 were a constant and contained no dynamics.

The parameterization $A(x) + B(x) \log_{10} Q^2 + C(x)(\log_{10} Q^2)^2$ has been used to fit the F_2 measurements at each value of x . The quality of the fit is good, and the result is shown in Figure 24 as solid lines. The constant W points on the parameterizations have been found according to the formula $W^2 = Q^2(1/x - 1)$, and are indicated on the plot with dashed lines. It is interesting to note the distortion in the fixed- W lines that occurs at $x \approx 10^{-4}$ at relatively high $Q^2 \approx 5 \text{ GeV}^2$ and at W above 85 GeV.

Since W at low x is related to x and Q^2 by $W^2 \approx Q^2/x$, the plot of $\partial F_2 / \partial \log Q^2$ at a constant W , over the Q^2 range covered by the data, should show a transition from the behavior according to Equation (4) to that of Equation (11), provided $xg(x, Q^2)$ has a weak Q^2 dependence and σ_0 , which corresponds to the photo-production cross-section, has a weak x (or equivalently energy) dependence. Since there is no quantitative prediction for the kinematic region in which the DGLAP formalism is applicable, the determination of the Q^2 and x at which this transition occurs is of great interest and may help in clarifying

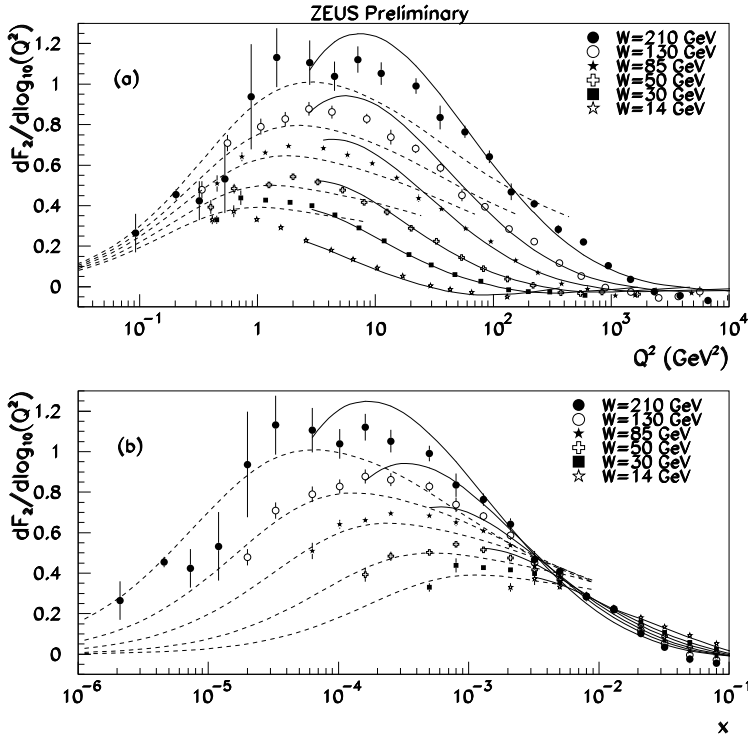


Figure 25: The logarithmic slope of F_2 at a constant W as a function of Q^2 and x . See text.

tion (11).

Figure 25b shows that at higher x , corresponding to higher Q^2 in Figure 25a, the derivatives fall with increasing x and tend to become independent of W at $x > 0.003$, in line with the expectation of Equation (4), if $xg(x, Q^2)$ has the form $x^{-\lambda}$ and only a slow dependence on Q^2 .

The value of Q^2 , or x , where the slope of the derivatives changes sign can be read off from Figures 25a and 25b.

This transition, for values of W above 85 GeV, happens at a relatively high Q^2 of 2-6 GeV^2 at the corresponding x of $5 \cdot 10^{-4}$ to $3 \cdot 10^{-3}$.

The dashed lines in Figure 25 are the prediction of the GB&W model, which explicitly incorporates the transition between the behaviors described in Equations (11) and (4) as a

In Figure 25, the derivatives of F_2 , evaluated from the fit $B + 2C \log_{10} Q^2$, are shown. The errors of the derivatives are evaluated using the errors on, and correlations between, the parameters B and C obtained from the polynomial fits. Figure 25a shows the derivatives at constant W as a function of Q^2 , whereas Figure 25b shows the same as a function of x .

Figure 25a shows that at lower Q^2 , corresponding to lower x in Figure 25b, the derivatives fall as Q^2 decreases and tend to become independent of W at Q^2 of about 0.4 GeV^2 . This is in line with the expectation of Equation

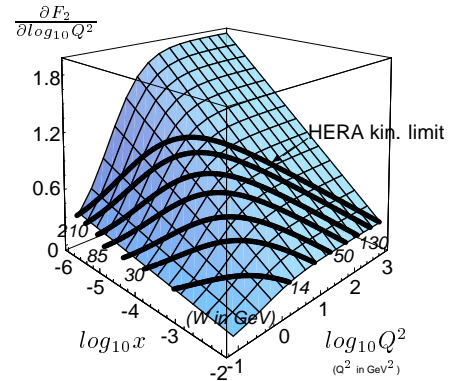


Figure 26: A schematic representation of Figure 25 in two dimensions. See text.

transition between the pQCD region and the saturation region of the dipole cross-section. The lines are drawn only at $x < 0.01$ where the model is applicable. The solid line is the result of a DGLAP fit by the ZEUS collaboration. The line is drawn only above $Q^2 > 2.7 \text{ GeV}^2$, where data have been fit. In case of the DGLAP fit, the peaking behavior of Figure 25 is related to the rapid decrease of the gluon density at low x between Q^2 of 10 GeV^2 and 1 GeV^2 [16, 37].

Figure 26 is a 2-dimensional visualization of the qualitative features of Figure 25. The lines of constant W (“trajectories”), plotted as thick solid lines, when projected to the Q^2 and x axes, approximately give Figures 22a and 22b, respectively. The peak structure of the constant W lines represents the transition from the region where $\partial F_2/\partial \log_{10} x$ is steeply rising with $-\log_{10} x$ to the region where it is steeply rising with $\log_{10} Q^2$, behaviors corresponding to Equations (4) and (11), respectively. The position of the peak structure does not depend strongly on the “trajectory”, $f(x, Q^2)$, at which the derivatives are plotted, chosen to be $W^2 \approx Q^2/x$ in Figure 25. Inspection of Figure 26 shows that almost any choice of a function $f(x, Q^2)$, which rises monotonically with decreasing x for a fixed Q^2 will have a peak at the same (x, Q^2) position which correctly indicates the transition. In particular, an early ZEUS analysis, made with a more limited data set available at the time, shows (Figure 27) the same transitional behavior at the same (x, Q^2) position.

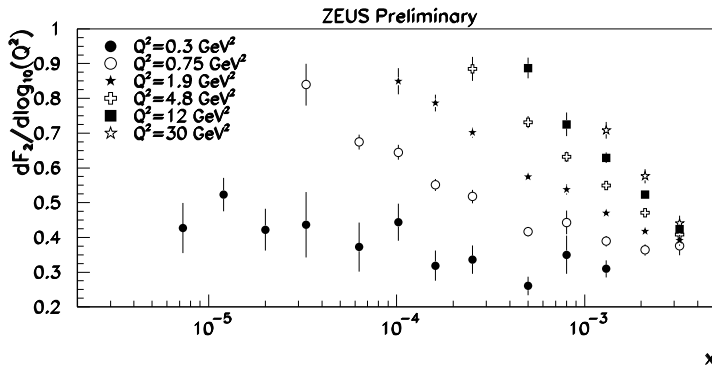


Figure 28: The logarithmic slope of F_2 for fixed Q^2 as a function of x .

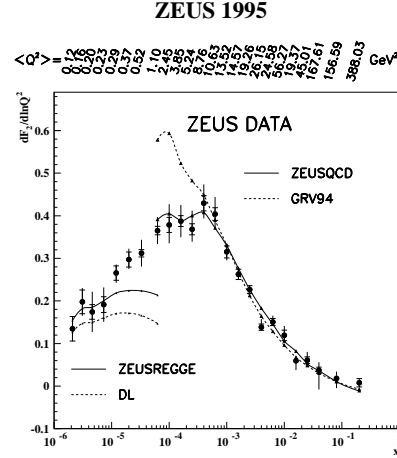


Figure 27: The logarithmic slope evaluated at Q^2 (scale at the top) and x (scale at the bottom). See text.

Figure 28 shows the derivatives plotted for constant Q^2 , as a function of x . At Q^2 above 1.9 GeV^2 , the derivatives rise rapidly as x decreases in line with the expectations of Equation (4) assuming $xg(x, Q^2)$ has the form $x^{-\lambda}$. As Q^2 falls, the rise of the derivative becomes less steep, as would be expected from Equation (11), if a mild energy

dependence, of the Regge type, is assumed for σ_0 ; thus a turn-over in Figure 28 is not expected from the GB&W model, while naively one might expect it from Equation (4) with saturating gluons, xg . The statements sometimes found in the literature that the turn-over found in Figure 27 is “accidental” or “only kinematic in origin” [33, 38, 39] arises from the combination of the expectation of a turn-over in Figure 28 as a manifestation of gluon saturation and the misunderstanding that Figure 27 is in some way an approximation of Figure 28; rather, it is an approximation of Figure 25.

5 Discussion and Outlook

The measurements of the proton structure at small x at HERA are now very precise. However, in spite of the expectation that these measurements should show some manifestation of dynamics beyond that incorporated in the $(\ln Q^2)$ expansion of the DGLAP formalism, the DGLAP fits to the data give a good description above Q^2 of about 1 GeV².

The question of whether the success of DGLAP fits merely indicates the flexibility of the parton parameterizations and the still-limited $(\ln Q^2)$ range of the measurement at small- x is not likely to be answered by looking at F_2 alone, at least in the currently available kinematic range. As discussed in Section 4, while the qualitative features of F_2 at small- x (and necessarily small Q^2), show some characteristics expected by a saturation model, the DGLAP fits can reproduce those same features without any parton saturation, as a result of a rapidly evolving gluon density at low Q^2 .

One of the most promising ways of investigating the small- x proton structure is to look at the inclusive DIS measurements together (“and” rather than “or” of the title) with the diffractive DIS reactions. While the theoretical understanding of the relation of small- x and diffraction is not yet very rigorous, the data sets from HERA provide many interesting indications of the underlying dynamics.

ACKNOWLEDGEMENTS

It is a pleasure to thank the organizers for a most enjoyable Symposium. The experimental results presented here are due to a huge collaborative effort, over many years, of the large number of people in the H1 and ZEUS experiments. I had many interesting discussions on the subject matter of this talk with many of my colleagues in H1 and ZEUS; I would particularly like to thank Brian Foster. I would also like to thank John Collins, Krzysztof Golec-Biernat, Al Mueller and Mara Soares for illuminating discussions. Finally, Jim Whitmore, Peter Schleper and Brian Foster were kind enough to carefully check the manuscript.

References

- [1] L. N. Lipatov, Sov. J. Nucl. Phys. **20**, 94 (1975);
V. N. Gribov and L. N. Lipatov, Sov. J. Nucl. Phys. **15**, 438 (1972);
G. Altarelli and G. Parisi, Nucl. Phys. **B126**, 298 (1977);
Y. L. Dokshitzer, Sov. Phys. JETP **46**, 641 (1977).
- [2] H. L. Lai *et al.*, Phys. Rev. **D 55**, 1280 (1997) [hep-ph/9606399].
- [3] C. Adloff *et al.* [H1 Collaboration], hep-ex/0012053.
- [4] ZEUS Collaboration, paper 412, XXXth International Conference on High Energy Physics, July 27–August 2, 2000, Osaka, Japan.
- [5] C. Adloff *et al.* [H1 Collaboration], Nucl. Phys. B **497**, 3 (1997) [hep-ex/9703012].
- [6] J. Breitweg *et al.* [ZEUS Collaboration], Eur. Phys. J. **C7**, 609 (1999) [hep-ex/9809005].
- [7] K. Prytz, Phys. Lett. B **311**, 286 (1993).
- [8] M. Derrick *et al.* [ZEUS Collaboration], Z. Phys. **C63**, 391 (1994);
S. Aid *et al.* [H1 Collaboration], Z. Phys. **C69**, 27 (1995) [hep-ex/9509001].
- [9] A. Donnachie and P. V. Landshoff, Nucl. Phys. **B231**, 189 (1984).
- [10] V. S. Fadin, E. A. Kuraev and L. N. Lipatov, Phys. Lett. **B60**, 50 (1975);
E. A. Kuraev, L. N. Lipatov and V. S. Fadin, Sov. Phys. JETP **44** (1976) 443;
E. A. Kuraev, L. N. Lipatov and V. S. Fadin, Sov. Phys. JETP **45** (1977) 199;
I. I. Balitsky and L. N. Lipatov, Sov. J. Nucl. Phys. **28**, 822 (1978).
- [11] V. S. Fadin and L. N. Lipatov, Phys. Lett. **B429**, 127 (1998) [hep-ph/9802290];
M. Ciafaloni and G. Camici, Phys. Lett. **B430**, 349 (1998) [hep-ph/9803389].
- [12] M. Ciafaloni, Nucl. Phys. **B296**, 49 (1988);
S. Catani, F. Fiorani and G. Marchesini, Nucl. Phys. **B336**, 18 (1990);
S. Catani, F. Fiorani and G. Marchesini, Phys. Lett. **B234**, 339 (1990).
- [13] L. V. Gribov, E. M. Levin and M. G. Ryskin, Phys. Rep. **100**, 1 (1983).
- [14] R. S. Thorne, Nucl. Phys. **B512**, 323 (1998) [hep-ph/9710541].
- [15] H. Jung, Nucl. Phys. Proc. Suppl. **79**, 429 (1999) [hep-ph/9905554].
- [16] J. Breitweg *et al.* [ZEUS Collaboration], Eur. Phys. J. **C6**, 43 (1999) [hep-ex/9807010].

- [17] C. Adloff *et al.* [H1 Collaboration], Z. Phys. **C76**, 613 (1997) [hep-ex/9708016].
- [18] H1 Collaboration, paper 571, XXIXth International Conference on High Energy Physics, July 23–29, 1998, Tampere, Finland.
- [19] J. C. Collins, Phys. Rev. **D 57**, 3051 (1998) [hep-ph/9709499].
- [20] G. Ingelman and P. E. Schlein, Phys. Lett. **B152**, 256 (1985).
- [21] C. Adloff *et al.* [H1 Collaboration], hep-ex/0012051.
- [22] K. Golec-Biernat and M. Wusthoff, Phys. Rev. **D 59**, 014017 (1999) [hep-ph/9807513].
- [23] K. Golec-Biernat and M. Wusthoff, Phys. Rev. **D 60**, 114023 (1999) [hep-ph/9903358].
- [24] E. Gotsman, E. Levin and U. Maor, Nucl. Phys. **B493**, 354 (1997) [hep-ph/9606280];
 E. Gotsman, E. Levin and U. Maor, Phys. Lett. **B425**, 369 (1998) [hep-ph/9712517];
 E. Gotsman, E. Levin, U. Maor and E. Naftali, Nucl. Phys. **B539**, 535 (1999) [hep-ph/9808257];
 N. N. Nikolaev and B. G. Zakharov, Z. Phys. **C49**, 607 (1991);
 N. Nikolaev and B. G. Zakharov, Z. Phys. **C53**, 331 (1992);
 V. Barone, M. Genovese, N. N. Nikolaev, E. Predazzi and B. G. Zakharov, Phys. Lett. **B326**, 161 (1994) [hep-ph/9307248];
 J. R. Forshaw, G. Kerley and G. Shaw, Phys. Rev. **D 60**, 074012 (1999) [hep-ph/9903341];
 W. Buchmuller, T. Gehrmann and A. Hebecker, Nucl. Phys. **B537**, 477 (1999) [hep-ph/9808454];
 A. H. Mueller and B. Patel, Nucl. Phys. **B425**, 471 (1994) [hep-ph/9403256];
 A. H. Mueller, Nucl. Phys. **B415**, 373 (1994).
 W. Buchmuller and A. Hebecker, Nucl. Phys. **B476**, 203 (1996) [hep-ph/9512329];
 W. Buchmuller, M. F. McDermott and A. Hebecker, Nucl. Phys. **B487**, 283 (1997) [hep-ph/9607290].
- [25] A. H. Mueller, hep-ph/9911289.
- [26] ZEUS Collaboration, paper 435, XXXth International Conference on High Energy Physics, July 27–August 2, 2000, Osaka, Japan.

- [27] C. Adloff *et al.* [H1 Collaboration], Phys. Lett. **B483**, 23 (2000) [hep-ex/0003020].
- [28] ZEUS Collaboration, paper 437, XXXth International Conference on High Energy Physics, July 27–August 2, 2000, Osaka, Japan.
- [29] ZEUS Collaboration, paper 438, XXXth International Conference on High Energy Physics, July 27–August 2, 2000, Osaka, Japan.
- [30] ZEUS Collaboration, paper 439, XXXth International Conference on High Energy Physics, July 27–August 2, 2000, Osaka, Japan.
- [31] A. C. Caldwell and M. S. Soares, hep-ph/0101085.
- [32] J. Bartels, J. Phys. **G26**, 481 (2000).
- [33] M. F. McDermott, hep-ph/0008260.
- [34] ZEUS Collaboration, paper 416, XXXth International Conference on High Energy Physics, July 27–August 2, 2000, Osaka, Japan.
- [35] M. R. Adams *et al.* [E665 Collaboration], Phys. Rev. **D 54**, 3006 (1996);
M. Arneodo *et al.* [New Muon Collaboration], Nucl. Phys. **B483**, 3 (1997) [hep-ph/9610231].
- [36] H. Abramowicz, E. M. Levin, A. Levy and U. Maor, Phys. Lett. **B269**, 465 (1991).
H. Abramowicz and A. Levy, hep-ph/9712415.
- [37] A. D. Martin, R. G. Roberts, W. J. Stirling and R. S. Thorne, Eur. Phys. J. **C4**, 463 (1998) [hep-ph/9803445].
- [38] E. Gotsman, Nucl. Phys. Proc. Suppl. **79**, 192 (1999).
- [39] A. De Roeck, in the Proceedings of “Yalta 2000, new trends in high-energy physics”.